

SUPPORTING INFORMATION

Designing yield stress fluids for advanced materials processing using derivatives of pH-responsive branched copolymer surfactants

Emma L. Jones,^{a,b} Zhidong Luo,^b Rishav Agrawal,^b Sean Flynn,^b Megan Carr,^c Will Sharratt,^b and Esther García-Tuñón^{*b,c}

^a*The Leverhulme Centre for Functional Materials Design, University of Liverpool, UK*

^b*School of Engineering, University of Liverpool, UK* ^b*Materials Innovation Factory, University of Liverpool, UK*

E-mail: egarcia@liverpool.ac.uk

December 6, 2024

1 Synthesis of BCS-derivatives: detailed example

In a typical synthesis of a highly branched BCS derivative, DDT-p(PEGMA_{2.0-co}-MAA_{8.0-co}-EGDMA_{0.8}), (S5), PEGMA ($M_n = 300 \text{ g mol}^{-1}$, 5.00 g, 0.017 mol, 2.0 eq.), MAA (5.739 g, 0.067 mol, 8.0 eq.), EGDMA (1.322 g, 1.259 mol, 0.8 eq.), DDT (1.687 g, 1.996 mmol, 1.0 eq.), AIBN (0.068 g, 0.417 mmol, 0.5 eq.) and EtOH (13.816 g, 50 wt% w.r.t. total mass) were added to an oven dried round bottomed flask containing a magnetic stirrer bar. The flask was sealed and purged with N₂ for 30 minutes before the addition of TMS (0.2 mL, stored under N₂). At this point an aliquot (ca. 100 μL , t_0) was withdrawn and diluted in MeOD for quantification of [PEGMA]₀:[MAA]₀ and [EGDMA]₀:[DDT]₀ by ¹H NMR spectroscopy. The flask was submerged in a preheated oil bath held at 70 °C and allowed to stir for 48 hours before the reaction was quenched by rapid cooling to 0 °C in an ice bath. Another aliquot (ca. 100 μL , t_f) was withdrawn to quantify monomer conversion by ¹H NMR. The solution was dried *in vacuo* and the resulting solid re-dissolved in the minimum amount of EtOH before being precipitated twice from EtOH into cold petroleum ether. This yielded DDT-p(PEGMA_{2.0-co}-MAA_{8.0-co}-EGDMA_{0.8}), (S5) as a viscous opaque oil. The polymer was dried *in vacuo* at 40 °C for 24 hours and characterised *via* ¹H NMR (MeOD) and TD-SEC using an MeOH (20 v/v%), sodium nitrate (0.05 M) and NaOH (0.004 M) eluent calibrated with pullulan and dextran multi-detector calibration.

2 ¹H NMR results

¹H NMR supporting data in figures SI1 and SI2 show how the peaks have been assigned and integrated. Overall monomer to chain transfer agent ratio ($\frac{[\text{PEGMA}]_0 + [\text{MAA}]_0 + [\text{EGDMA}]_0}{[\text{DDT}]_0}$), bifunctional monomer to chain transfer agent ratio ($\frac{[\text{EGDMA}]_0}{[\text{DDT}]_0}$) and ratio of PEGMA to MMA ($\frac{[\text{PEGMA}]_0}{[\text{PEGMA}]_0 + [\text{MAA}]_0}$) were determined from integral values of their corresponding NMR signals, normalised to 1 proton. For example, vinyl resonances were used without further scaling whereas the integral of the EGDMA CH₂ at ~ 4.4 ppm was divided by 4, PEGMA CH₂ at ~ 4.3 ppm by 2, and the integral of the DDT CH₂ at ~ 2.5 ppm by 2. Conversion was determined from the integrals of the vinyl resonances for the initial (t_0) and final (after 24 hour) reactions mixtures (t_f):

$$\text{Conversion}(\%) = 100 \times \left(1 - \frac{\int_{6.05}^{6.15} \delta_{t_f}}{\int_{6.05}^{6.15} \delta_{t_0}} \right) \quad (1)$$

3 Powder Characterisation Results

Here we include all the curated results obtained from the characterisation of powder properties for both, activated charcoal (AC, figures 4 and 5) and strontium titanate (SrTiO_3 , STO, figures 6 and 7). A summary of these results is included in the captions as appropriate.

4 Mathematical frameworks used in the LAOS analysis of transient data

4.1 Fourier-Transform (FT) rheology

For a sinusoidal strain input $\gamma(t) = \gamma_0 \sin(\omega t)$, the stress response can be represented by a Fourier series:^{1,2}

$$\sigma(t; \omega, \gamma_0) = \gamma_0 \sum_{n \text{ odd}} \left\{ G'_n(\omega, \gamma_0) \sin(n\omega t) + G''_n(\omega, \gamma_0) \cos(n\omega t) \right\}. \quad (2)$$

In the linear viscoelastic regime (LVR), the stress response includes only the first-harmonic, $n = 1$. Based on symmetry arguments, the stress response that remains unchanged if the coordinate system is reversed, will result in only odd harmonics in the Fourier series representation.^{3,4} Even harmonics are commonly related to nonperiodic or asymmetric slip/yield responses.⁴

4.2 Lissajous-Bowditch (LB) curves, and plastic dissipation ratio

In a LAOS experiment, the material's instantaneous properties over the entire oscillation can be visualized using the elastic and viscous LB projections. The shape of the elastic LB curves provides visual information about how the material responds during an amplitude sweep. At small strain amplitudes, a straight line corresponds to purely elastic and a circle to purely viscous; while a rectangle shape at large strain amplitudes corresponds to a perfect plastic behaviour. The distortion of LB curves evidence the raising of non-linear behaviours, while the area within the curve represents the energy being dissipated. The visual information provided by these curves is quantified using the plastic dissipation ratio, ϕ . This is the ratio of the energy dissipated in a single oscillation cycle (area enclosed in a elastic LB curve, E_d) to the energy that would be dissipated in a perfect plastic response (which would correspond to a in the elastic LB curves) with equivalent strain amplitude and maximum stress ($(E_d)_{pp}$),⁴

$$\phi = \frac{E_d}{(E_d)_{pp}}. \quad (3)$$

A perfect plastic behaviour corresponds to $\phi = 1$ and a purely elastic response to $\phi = 0$.

4.3 Sequence of physical processes (SPP)

The Sequence of physical processes (SPP) approach has been developed by Rogers and co-workers⁵⁻⁸ providing new insights on the time dependency of the non-linear rheological behaviours. This technique provides quantitative information for all strain, strain rate, and stress points along the LB curves. It utilizes the Frenet-Serret theorem,⁹ which defines the motion of a moving particle along a curvature with three orthonormal set of vectors direction: the tangent vector ($\mathbf{T}(t)$) pointing in the direction of the motion, the normal vector ($\mathbf{N}(t)$) pointing to the centre of the curvature of the motion, and the binormal vector ($\mathbf{B}(t)$) pointing normal to both $\mathbf{T}(t)$ and $\mathbf{N}(t)$. Each point throughout the LB curve is given by the position vector $\mathbf{P}(t) = [\gamma(t), \dot{\gamma}(t), \sigma(t)]$, and therefore the three orthonormal vectors are given by,

$$\mathbf{T}(t) = \frac{\mathbf{P}'(t)}{|\mathbf{P}'(t)|}, \quad \mathbf{N}(t) = \frac{\mathbf{T}'(t)}{|\mathbf{T}'(t)|}, \quad \mathbf{B}(t) = \mathbf{T}(t) \times \mathbf{N}(t). \quad (4)$$

The projections of the binormal vector $\mathbf{B}(t) = (B_\gamma, B_{\dot{\gamma}/\omega}, B_\sigma)$ and the orientation of the osculating plane at every point in the LB curves are then used to calculate the transient elastic modulus (G'_t) which quantifies change in stress w.r.t. strain, and transient viscous modulus (G''_t) which quantifies change in stress w.r.t. strain rate,^{10,11}

$$G'_t = -\frac{B_\gamma}{B_\sigma} = \frac{\partial \sigma}{\partial \gamma}, \quad (5)$$

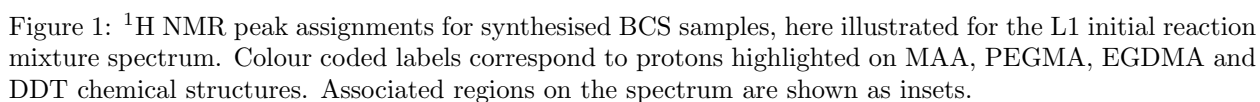
$$G''_t = -\frac{B_{\dot{\gamma}/\omega}}{B_\sigma} = \frac{\partial \sigma}{\partial (\frac{\dot{\gamma}}{\omega})}. \quad (6)$$

If $G'_t > G''_t$, the material behaviour is predominantly elastic or ‘solid-like’, and if $G''_t > G'_t$ the material behaviour is predominantly viscous or ‘liquid-like’.

In SPP analysis, the rheological transition within an oscillation cycle is generally investigated using a transient Cole–Cole plot.^{5,11–14} The Cole–Cole plot can be viewed as a trajectory of a point with coordinates G'_t (transient elastic modulus) and G''_t (transient viscous modulus) in the horizontal and vertical directions, respectively. By examining the trace of G'_t and G''_t in the Cole–Cole plot, one may determine the rheological transition in a particular range of interest.⁵ Strain softening or hardening is associated with sideways movements to the left or right, respectively. Shear thinning or thickening is associated with motion to the top or bottom, respectively. The location of the material response in the $[G'_t \ G''_t]$ - space also provides additional information. $G''_t = 0$ corresponds to purely elastic response, whereas $G'_t = 0$ corresponds to purely viscous response. When $G''_t > G'_t$, a response would be said to be predominantly viscous, while $G''_t < G'_t$ would be described as a predominantly elastic response. A transition from a predominantly elastic to a predominantly viscous response indicates fluidization, whereas from a predominantly viscous to a predominantly elastic response indicates solidification. $G'_t < 0$ represents a recoil process, whereas $G''_t < 0$ represents backflow of material.⁵ The raw waveforms data i.e. $\sigma(t)$, $\gamma(t)$ and $\dot{\gamma}(t)$ are analyzed using SPP freeware for MATLAB provided by its developers (<https://publish.illinois.edu/rogerssoftmatter/freeware/>). The SPP analysis is carried out in one full-cycle using Fourier domain filtering, where first 19 harmonics are used to reconstruct the stress waveform.

5 Rheology Results

The LAOS fingerprints for the M-series are included in the main text. Here we include the LAOS fingerprints for the S-series (figure 8) and L-series (figure 9) formulations: AC suspensions, and STO emulsified suspensions (measured after triggering the assembly of the correspondent BCS-derivative using G δ L).



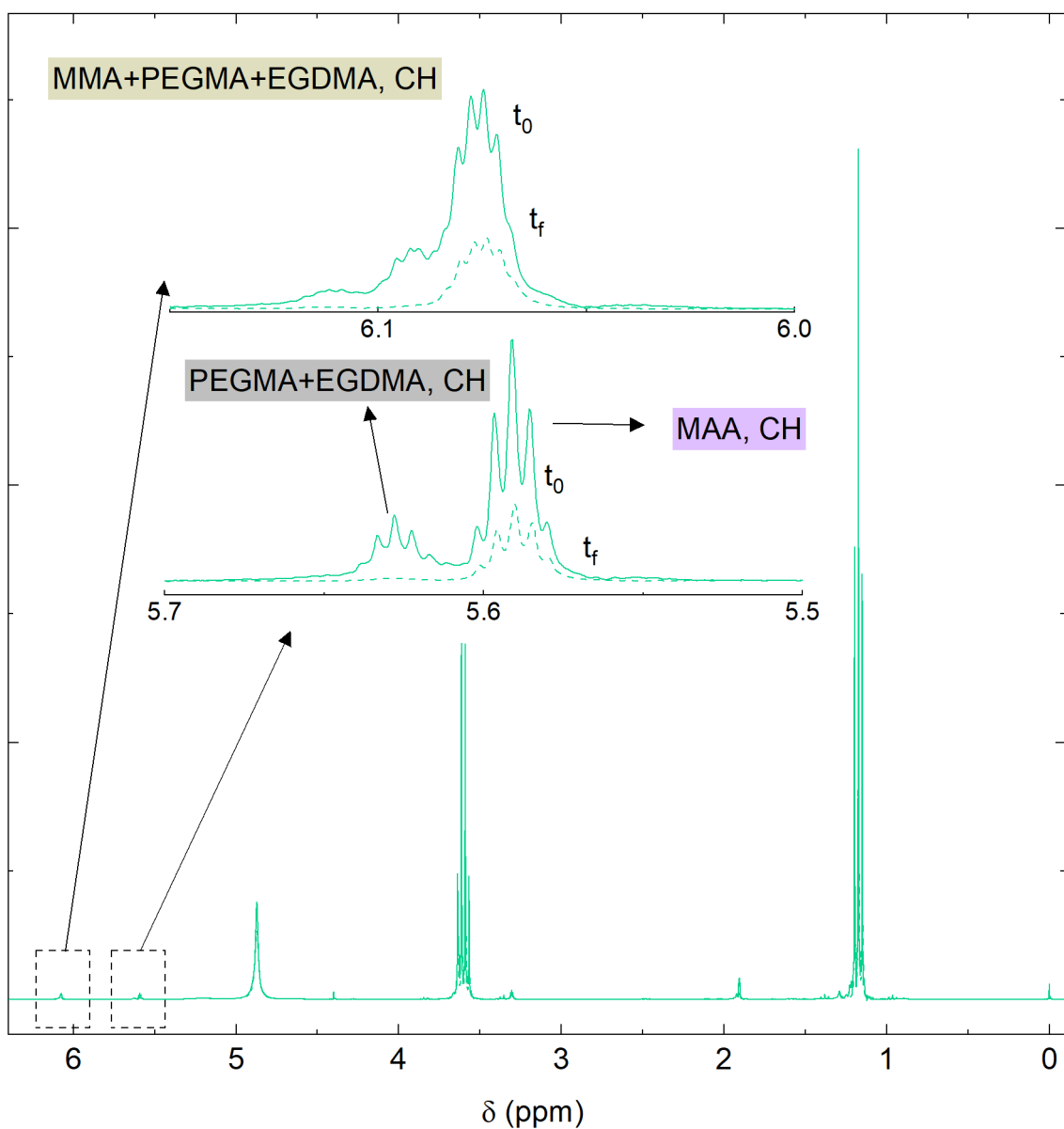


Figure 2: Overlaid ^1H NMR spectra for L1, here illustrated for the L1 spectrum. Colour coded labels correspond to protons highlighted on MMA, PEGMA, EGDMA and DDT chemical structures. Associated regions on the spectrum are shown as insets.

References

- [1] M. Wilhelm, *Macromolecular materials and engineering*, 2002, **287**, 83–105.
- [2] J. M. Dealy and K. F. Wissbrun, *Melt rheology and its role in plastics processing: theory and applications*, Springer Science & Business Media, 2012.
- [3] R. B. Bird, C. F. Curtiss, R. C. Armstrong and O. Hassager, *Dynamics of polymeric liquids, volume 2: Kinetic theory*, Wiley, 1987.
- [4] R. H. Ewoldt, P. Winter, J. Maxey and G. H. McKinley, *Rheologica acta*, 2010, **49**, 191–212.
- [5] S. A. Rogers, *Rheologica Acta*, 2017, **56**, 501–525.
- [6] S. A. Rogers, B. M. Erwin, D. Vlassopoulos and M. Cloitre, *J. Rheol.*, 2011, **55**, 435–458.

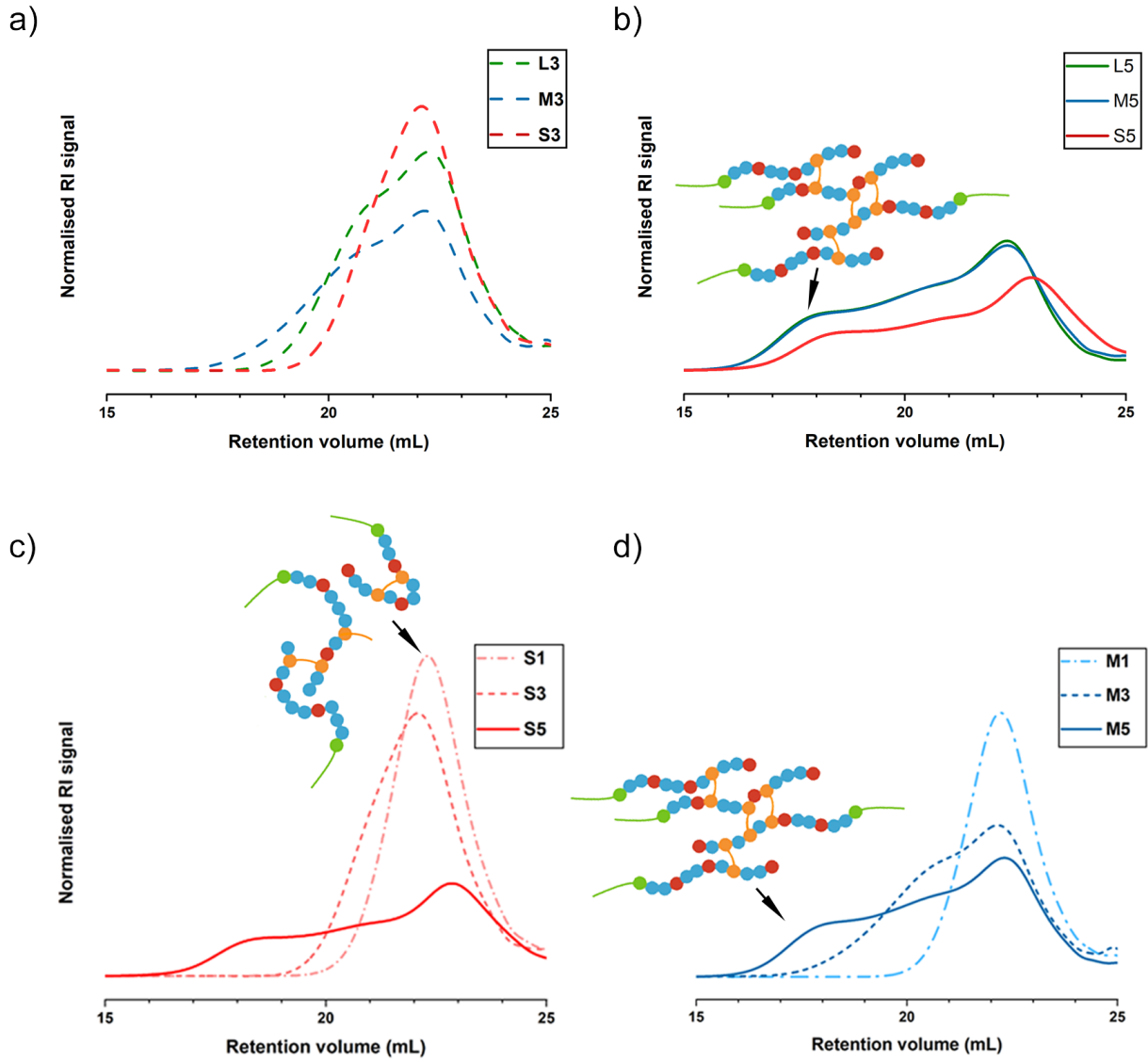


Figure 3: TD-GPC traces. Overlaid graphs showing the impact of longer PEGMA chain length (S, M and L) at a solids concentration of 30 wt% (a) and 30 wt% (b). And overlaid results for fixed PEGMA length S (c) and M (d) with increasing solids concentration in the reaction environment. High dilution results in linear polymers with broad mono-modal peaks. When the solids concentration increases, branching is favoured.

- [7] S. A. Rogers and M. P. Lettinga, *Journal of rheology*, 2012, **56**, 1–25.
- [8] C.-W. Lee and S. A. Rogers, *Korea-Australia Rheology Journal*, 2017, **29**, 269–279.
- [9] A. N. Pressley, *Elementary differential geometry*, Springer Science & Business Media, 2010.
- [10] J. D. Park and S. A. Rogers, *Physics of Fluids*, 2020, **32**, year.
- [11] M. Y. Erturk, S. A. Rogers and J. Kokini, *Food Hydrocolloids*, 2022, **128**, 107558.
- [12] G. J. Donley, J. R. de Bruyn, G. H. McKinley and S. A. Rogers, *Journal of Non-Newtonian Fluid Mechanics*, 2019, **264**, 117–134.
- [13] Y. Kim, S. Kim, B. S. Kim, J. H. Park, K. H. Ahn and J. D. Park, *Physics of Fluids*, 2022, **34**, year.
- [14] A. M. Le, M. Y. Erturk and J. Kokini, *Journal of Food Engineering*, 2023, **336**, 111193.

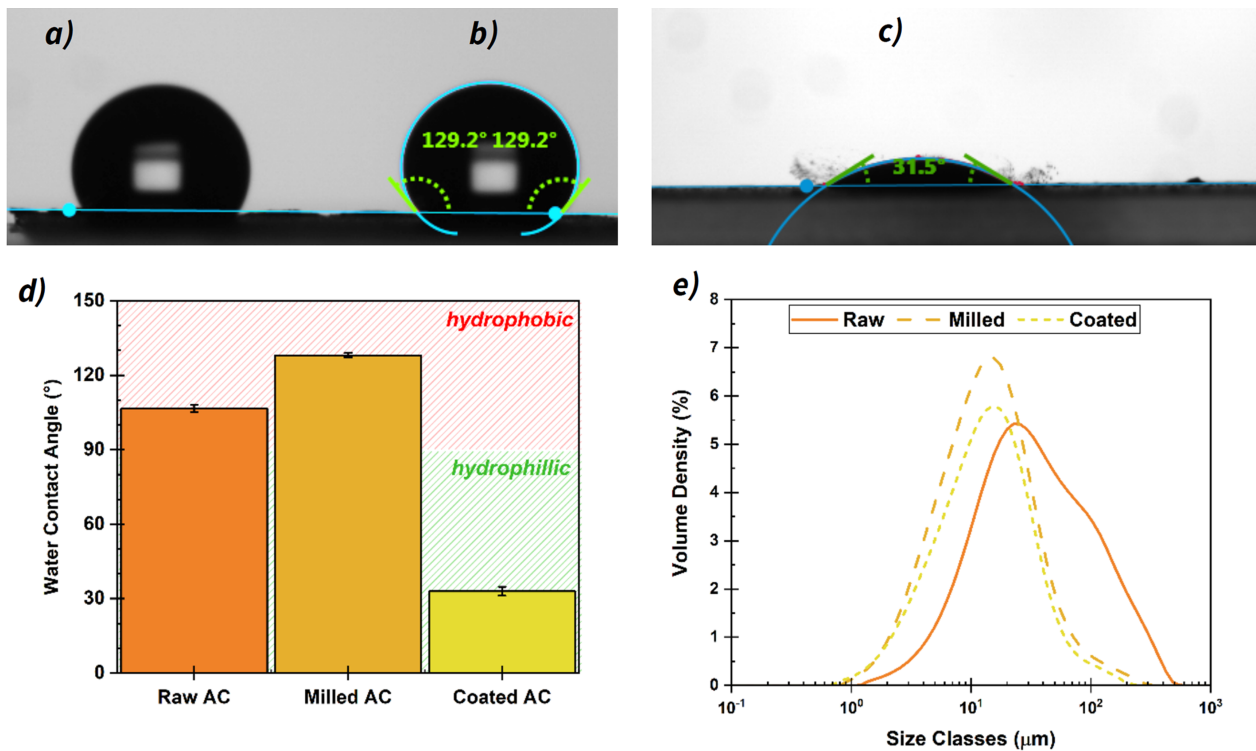


Figure 4: Contact angle (a-d) and particle size distribution (e) results for activated charcoal. The histogram in (c) and graph in (d) show a comparison of the results for the as-received material (raw), after dry milling and after stabilisation with BCSL1. The images (a-c) measurements evidence the considerable decrease when the powders are coated with BCSs. Milling and BCS stabilisation facilitate the reduction of particle size and the break down of agglomerates.

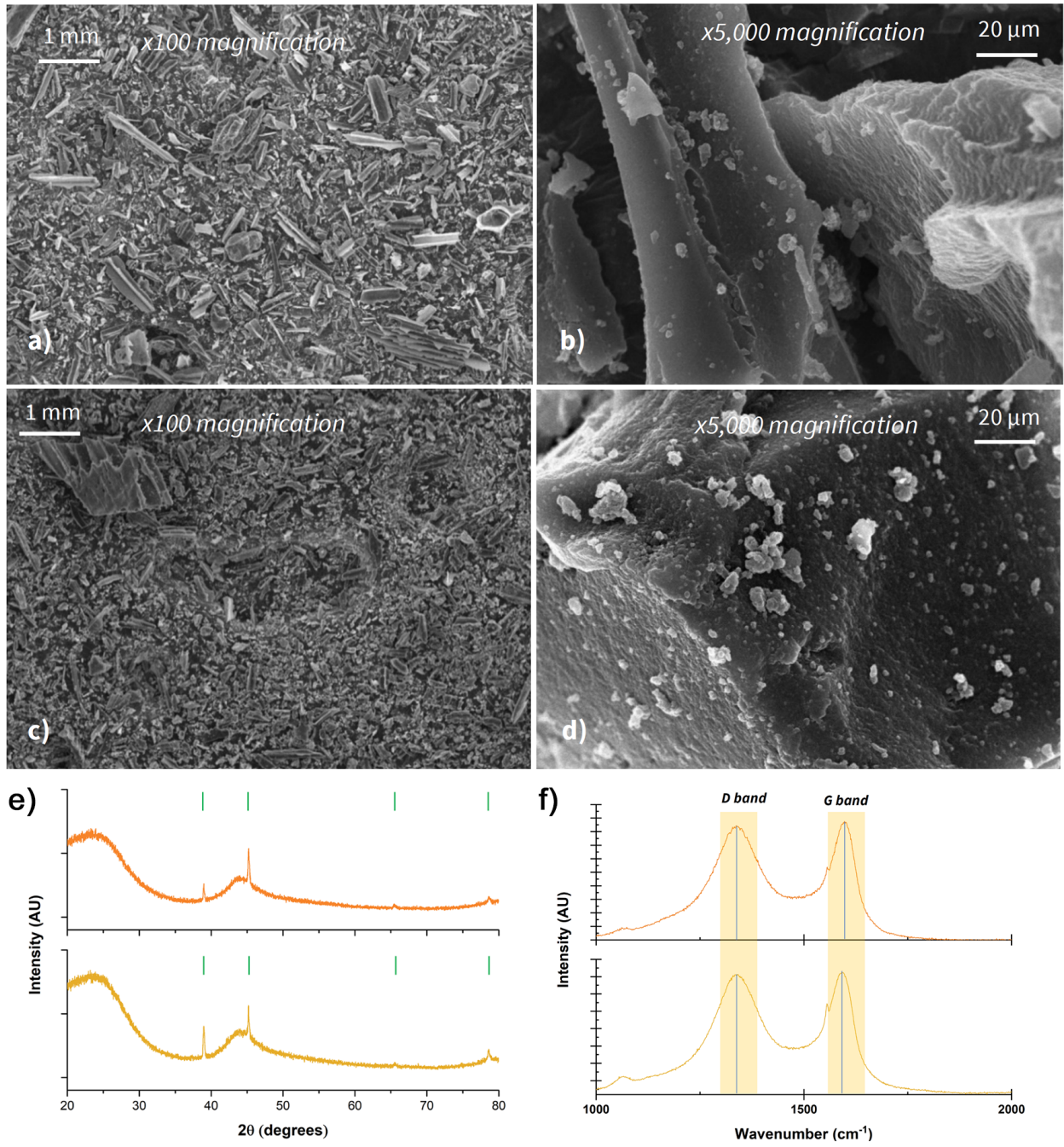


Figure 5: (a-d) SEM images showing the morphology of AC particles before and after dry milling. The images provide additional evidence of the wide particle size distribution. XRD and Raman analyses showing characteristic diffraction peaks and vibrational bands for AC, before processing (bottom) and after post-processing (top).

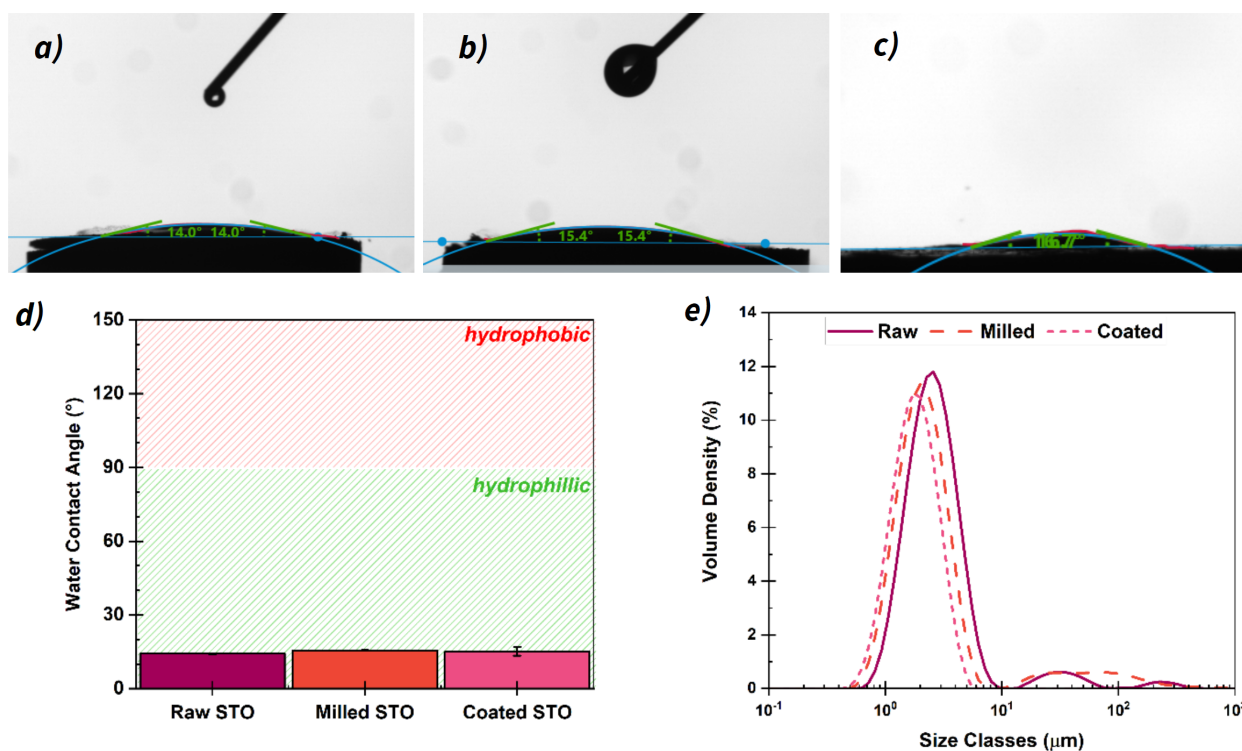


Figure 6: (a-d) Water contact angle and (e) particle size distribution results for STO powders as received (raw), after milling and after BCS surface functionalisation. STO particles are hydrophilic. BCS molecules aid the dispersion and stabilisation of STO particles, evidenced by the reduction of aggregates with sizes above 10 μm .

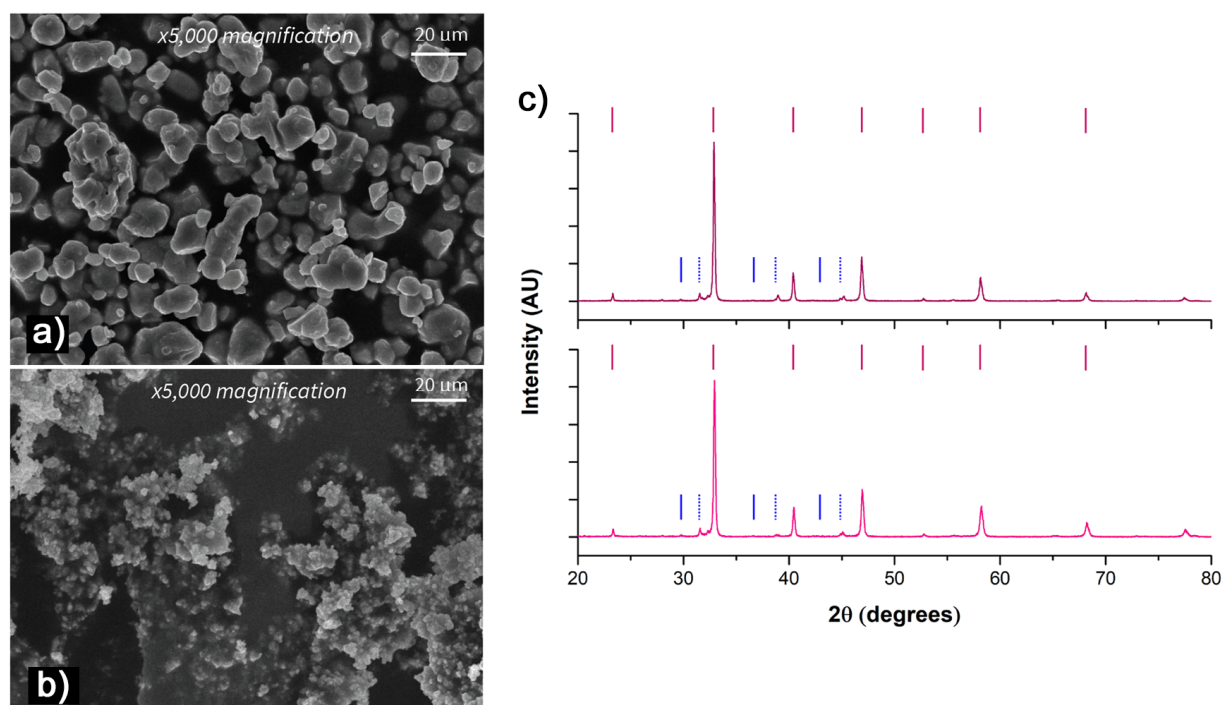


Figure 7: (a-b) SEM images of STO powders before and after milling. (c) XRD results for STO confirming the preservation of the crystalline structure before processing (bottom) and after post-processing (top).

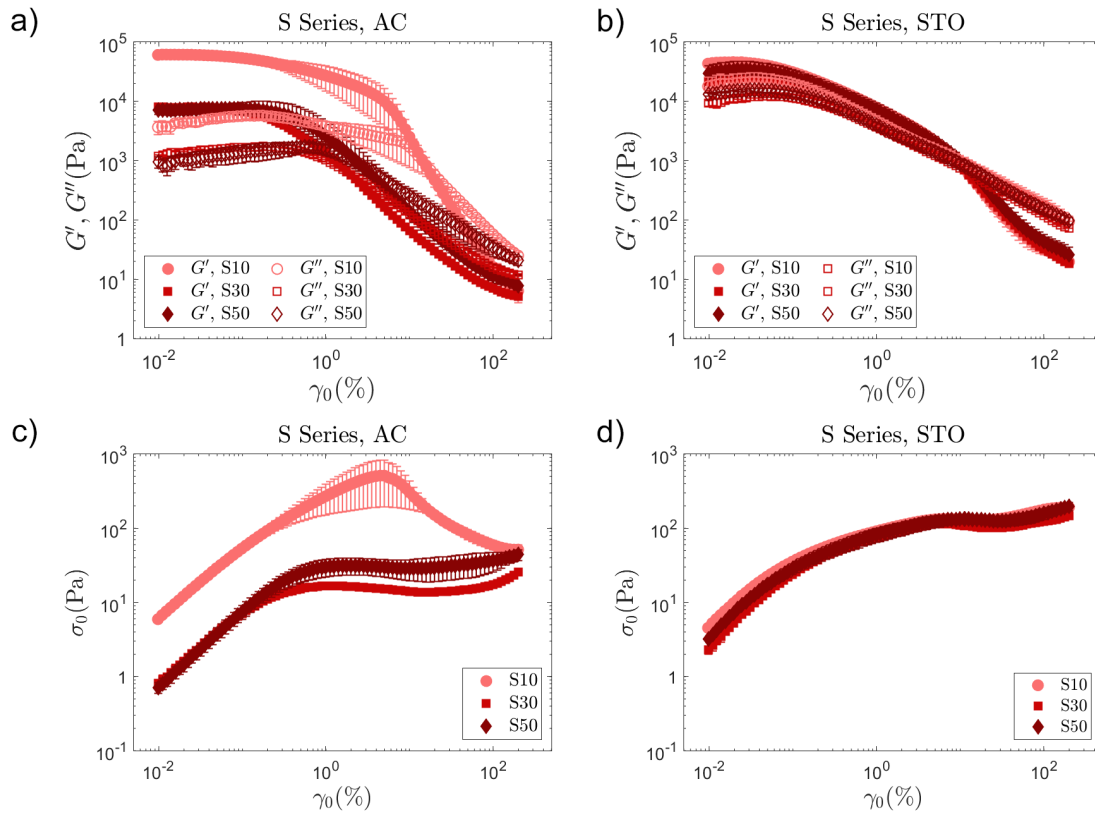


Figure 8: LAOS results for the S-series showing the moduli (G' and G'') evolution with strain amplitude (γ_0) for AC (a) and STO (b). σ_0 vs γ_0 graphs, showing an intense overshoot for the sample S1.

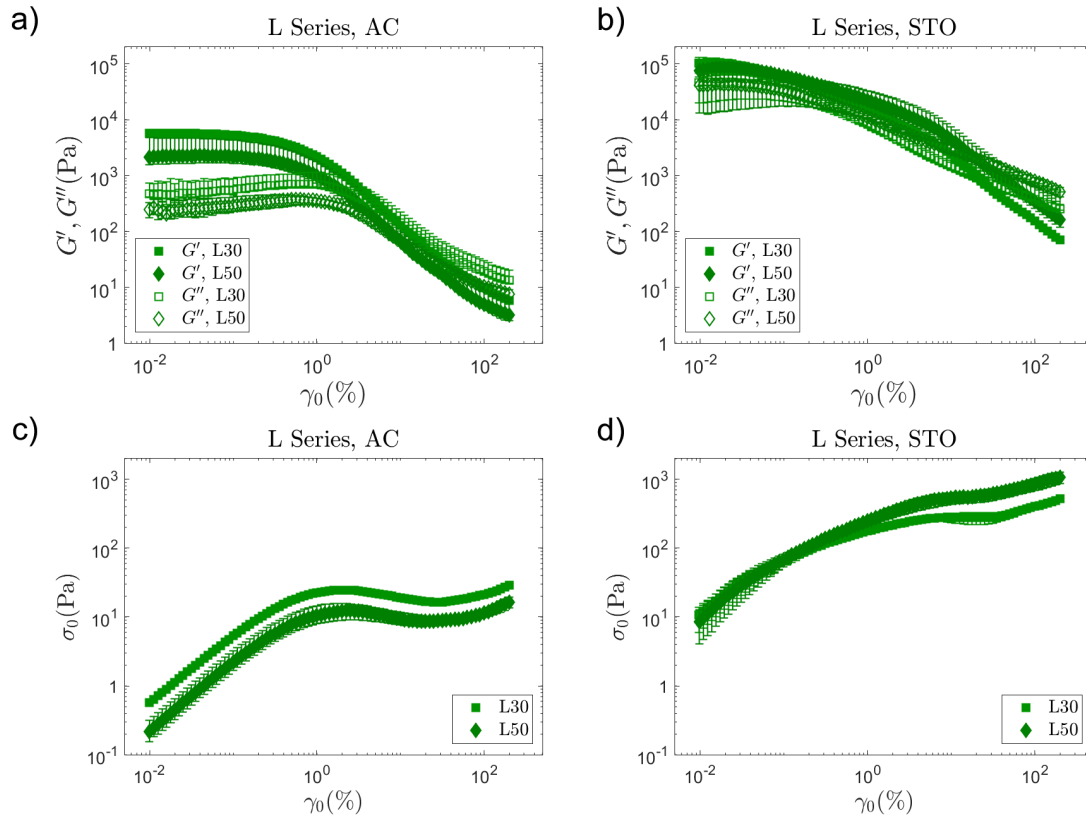


Figure 9: LAOS results for the L-series showing the moduli (G' and G'') evolution with strain amplitude (γ_0) for AC (a) and STO (b). σ_0 vs γ_0 graphs. The results show better consistency between repeats for both materials.



Figure 10: Adding G δ L to a stable STO emulsion gel (to trigger a controlled assembly through inter macro-molecular hydrogen bond formation) leads to a very heterogeneous formulations with signs of microstructure disruption (e.g. phase separation, aggregates and macroscopic cracks).

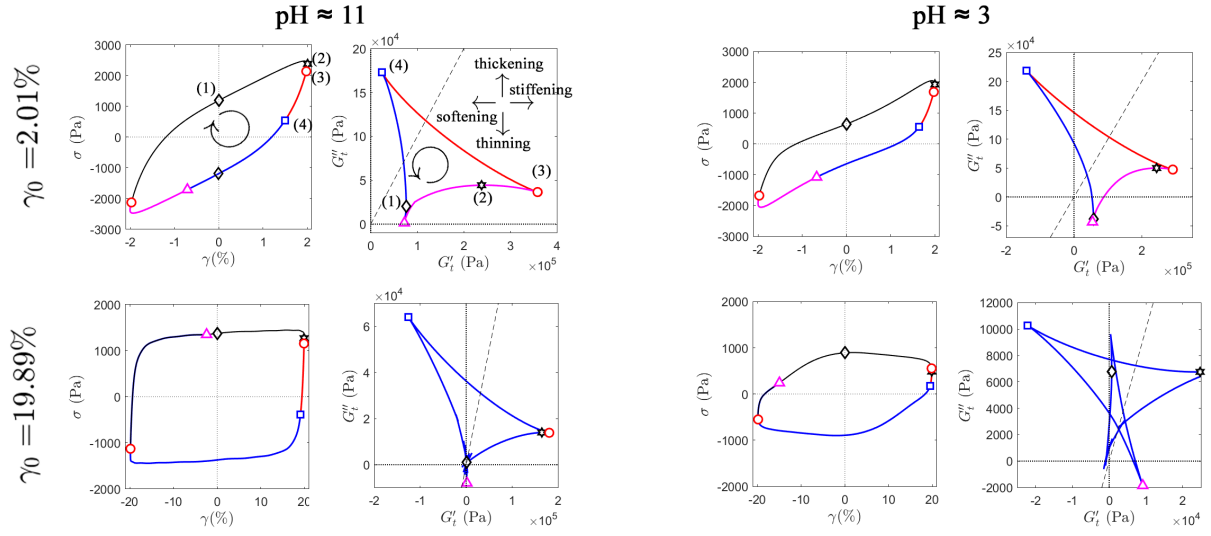


Figure 11: Elastic Lissajous plots and Cole-Cole plots for selected representative strains $\gamma_0 \approx 2\%$ and $\gamma_0 \approx 20\%$ for the emulsion gel at $\text{pH} \approx 11$ and the disrupted gel at $\text{pH} \approx 3$. The SPP intra-cycle trajectory at $\gamma_0 \approx 2\%$ shows that the disrupted gel undergoes a greater deformation at the same strain amplitude, entering the recoil and backflow regions. For this sample ($\text{pH} \approx 3$), increasing the strain amplitude from 0 to $\gamma_0 \approx 2\%$ leads to simultaneous stiffening and thickening (increase of both G'_t and G''_t). As γ_0 decreases, the sample softens and thickens (square), and then continues to thin and stiffen simultaneously. Both samples undergo very different processes in the cycle at any strain within the flow transition. At large amplitude, e.g. $\gamma_0 \approx 20\%$, the disrupted gel shows intense non-linearities and strange transitions in the Cole-Cole plot that likely do not have any physical meaning given the extensive damage of the microstructure.